BUMPS IN SMALL-WORLD NETWORKS

CARLO R. LAING

Abstract. We consider a network of coupled excitatory and inhibitory theta neurons which is capable of supporting stable spatially-localised "bump" solutions. We randomly add long-range and simultaneously remove short-range connections within the network to form a small-world network and investigate the effects of this rewiring on the existence and stability of the bump solution. We consider two limits in which continuum equations can be derived; bump solutions are *fixed points* of these equations. We can thus use standard numerical bifurcation analysis to determine the stability of these bumps and to follow them as parameters (such as rewiring probabilities) are varied. We find that under some rewiring schemes bumps are quite robust, whereas in other schemes they can become unstable via Hopf bifurcation or even be destroyed in saddle-node bifurcations.

1. Introduction

Spatially-localised "bumps" of activity in neuronal networks have been studied for many years, as they are thought to play a role in short term memory [13, 53, 10, 12] and the head direction system [54, 43], among other phenomena. Some models of bump formation have used a firing rate description [52, 3, 20, 39, 29] while others have considered networks of spiking neurons [30, 19, 48]. The simplest models typically have "Mexican-hat" connectivity in a single population of neurons, where nearby neurons are excitatorily coupled and more distant ones are inhibitorily coupled [10, 15]. However, more realistic models consider both excitatory and inhibitory neurons with non-negative connectivity within and between populations [6, 41]. Almost all previous models have considered homogeneous and isotropic networks, which typically support a continuous family of reflection-symmetric bumps, parametrised by their position in the network. Some exceptions are [9, 8], in which a spatially-inhomogeneous coupling function is used, and [47], in which a spatially-varying random firing threshold is imposed.

In this paper we further investigate the effects of breaking the spatial homogeneity of neural networks which support bump solutions, by randomly adding long-range connections and simultaneously removing short-range connections in a particular formulation of small-world networks [45]. Small-world networks [51] have been much studied and there is evidence for the existence of small-worldness in several brain networks [11]. In particular, we are interested in determining how sensitive networks which support bumps are to this type of random rewiring of conections, and thus how precisely networks must be constructed in order to support bumps.

We will consider networks of heterogeneous excitatory and inhibitory theta neurons, the theta neuron being the canonical model for a Type I neuron for which the onset of firing is through a saddle-node on an invariant circle bifurcation [16, 18]. In several limits such networks are amenable to the use of the Ott/Antonsen ansatz [36, 37], and we will build on previous work using this ansatz in the study of networks of heterogeneous theta neurons [22, 24, 31, 44]. We present the model in Sec. 2.2 and then

Date: May 20, 2016.

Key words and phrases. Ott/Antonsen, theta neuron, bump, small-world, working memory, bifurcation.

consider two limiting cases: an infinite number of neurons (Sec. 2.3) and an infinite ensemble of finite networks with the same connectivity (Sec. 2.4). Results are given in Sec. 3 and we conclude in Sec. 4. Appendix A contains some mathematical manipulations relating to Sec. 2.4.

2. Materials and Methods

2.1. **Introduction.** First consider an all-to-all coupled network of N heterogeneous theta neurons whose dynamics are given by

$$\frac{d\theta_i}{dt} = 1 - \cos\theta_i + (1+\cos\theta_i)(I_i + gr) \tag{1}$$

$$\tau\frac{dr}{dt} = \frac{1}{N}\sum_{j=1}^{N} P_n(\theta_j) - r \tag{2}$$

for $i = 1, 2, \dots N$ where $\theta_i \in [0, 2\pi)$ is the phase of the ith neuron, $P_n(\theta) = a_n(1-\cos\theta)^n, n \in \mathbb{N}^+$ and a_n is a normalisation factor such that $\int_0^{2\pi} P_n(\theta)d\theta = 2\pi$. The function P_n is meant to mimic the action potential generated when a neuron fires, i.e. its phase increases through π; n controls the "sharpness" of this function. The I_i are input currents randomly chosen from some distribution, g is the strength of connectivity within the network (positive for excitatory coupling and negative for inhibitory), and τ is a time constant governing the synaptic dynamics. The variable r is driven up by spiking activity and exponentially decays to zero in the absence of activity, on a timescale τ.

The model (1)-(2) with $\tau = 0$ (i.e. instantaneous synapses) was studied by [31], who found multistability and oscillatory behaviour. The case of $\tau > 0$ was considered in [26] and similar forms of synaptic dynamics have been considered elsewhere [17, 7, 14]. The model presented below results from generalising (1)-(2) in several ways. Firstly, we consider two populations of neurons, one excitatory and one inhibitory. Thus we will have two sets of variables, one for each population. Such a pair of interacting populations was previously considered by [14, 25, 32, 7]. Secondly, we consider a spatially-extended network, in which both the excitatory and inhibitory neurons lie on a ring, and are (initially) coupled to a fixed number of neurons either side of them. Networks with similar structure have been studied by many authors [13, 19, 22, 24, 30, 43].

2.2. **Model.** We consider a network of $2N$ theta neurons, N excitatory and N inhibitory. Within each population the neurons are arranged in a ring, and there are synaptic connections between and within populations, whose strength depends on the distance between neurons, as in [27, 19]. (In the networks we will consider, connection strengths are either 1 or 0, i.e. neurons are either connected or not connected.) Inhibitory synapses act on a timescale τ_i, whereas the excitatory ones act on a timescale τ. $\theta_i \in [0, 2\pi)$ is the phase of the ith excitatory neuron and $\phi_i \in [0, 2\pi)$ is the phase of the ith inhibitory

one. The equations are

$$\frac{d\theta_i}{dt} = 1 - \cos\theta_i + (1+\cos\theta_i)(I_i + g_{EE}v_i - g_{EI}y_i) \tag{3}$$

$$\frac{d\phi_i}{dt} = 1 - \cos\phi_i + (1+\cos\phi_i)(J_i + g_{IE}u_i - g_{II}z_i) \tag{4}$$

$$\tau\frac{dv_i}{dt} = r_i - v_i \tag{5}$$

$$\tau\frac{du_i}{dt} = q_i - u_i \tag{6}$$

$$\tau_i\frac{dy_i}{dt} = s_i - y_i \tag{7}$$

$$\tau_i\frac{dz_i}{dt} = w_i - z_i \tag{8}$$

for $i = 1, 2 \dots N$, where

$$q_i = \frac{1}{N}\sum_{j=-M_{IE}}^{M_{IE}} P_n(\theta_{i+j}) \tag{9}$$

$$r_i = \frac{1}{N}\sum_{j=-M_{EE}}^{M_{EE}} P_n(\theta_{i+j}) \tag{10}$$

$$s_i = \frac{1}{N}\sum_{j=-M_{EI}}^{M_{EI}} P_n(\phi_{i+j}) \tag{11}$$

$$w_i = \frac{1}{N}\sum_{j=-M_{II}}^{M_{II}} P_n(\phi_{i+j}) \tag{12}$$

where P_n is as in Sec. 2.1. The positive integers M_{IE}, M_{EE}, M_{EI} and M_{II} give the width of connectivity from excitatory to inhibitory, excitatory to excitatory, inhibitory to excitatory, and inhibitory to inhibitory populations, respectively. The non-negative quantities g_{EE}, g_{EI}, g_{IE} and g_{II} give the overall connection strengths within and between the two populations (excitatory to excitatory, inhibitory to excitatory, excitatory to inhibitory, and inhibitory to inhibitory, respectively). The variable v_i (when multiplied by g_{EE}) gives the excitatory input to the ith excitatory neuron, and whose dynamics are driven by r_i, which depends on the activity of the excitatory neurons with indices between $i - M_{EE}$ and $i + M_{EE}$. Similarly, u_i (when multiplied by g_{IE}) gives the excitatory input to the ith inhibitory neuron, and is driven by q_i, which depends on the activity of the excitatory neurons with indices between $i - M_{IE}$ and $i + M_{IE}$. $g_{EI}y_i$ is the inhibitory input to the ith excitatory neuron, driven by s_i, which depends on the activity of the inhibitory neurons with indices between $i - M_{EI}$ and $i + M_{EI}$. Lastly, $g_{II}z_i$ is the inhibitory input to the ith inhibitory neuron, driven by w_i, which depends on the activity of the inhibitory neurons with indices between $i - M_{II}$ and $i + M_{II}$.

For simplicity, and motivated by the results in [41], we assume that the inhibitory synapses act instantaneously, i.e. $\tau_i = 0$, and that there are no connections within the inhibitory population, i.e. $g_{II} = 0$. Thus (8) and (12) become irrelevant and from (7) we have that $y_i = s_i$ in (3).

The networks are made heterogeneous by randomly choosing the currents I_i from the Lorentzian

$$h(I) = \frac{\Delta/\pi}{(I - I_0)^2 + \Delta^2} \tag{13}$$

and the currents J_i from the Lorentzian

$$g(J) = \frac{\Delta/\pi}{(J-J_0)^2+\Delta^2}. \tag{14}$$

I_0 and J_0 are the centres of these distributions, and for simplicity we assume that both have the same width, Δ. The heterogeneity of the neurons (i.e. the positive value of Δ) is not necessary in order for the network to support bumps, but it is necessary for the Ott/Antonsen ansatz, used extensively below, to be valid [38]. Networks of *identical* phase oscillators are known to show non-generic behaviour which can be studied using the Watanabe/Strogatz ansatz [50, 49]. We want to avoid non-generic behaviour, and having a heterogeneous network is also more realistic. For typical parameter values we see the behaviour shown in Figs. 1 and 2, i.e. a stable stationary bump in which the active neurons are spatially localised.

(While these bumps may look superficially like "chimera" states in a ring of oscillators [21, 1, 2, 40] they are different in one important aspect. Chimera states in the references above occur in networks for which the dynamics depend on only *phase differences.* Thus these systems are invariant with respect to adding the same constant to all oscillator phases, and can be studied in a rotating coordinate frame in which the synchronous oscillators have zero frequency, i.e. only *relative* frequencies are meaningful. In contrast, networks of theta neurons like those studied here are *not* invariant with respect to adding the same constant to all oscillator phases. The actual value of phase matters, and the neurons with zero frequency in Fig. 2 have zero frequency simply because their input is not large enough to cause them to fire.)

We now want to introduce rewiring parameters in such a way that on average, the number of connections is preserved as the networks are rewired. This is different from other formulations of small-world networks in which additional edges are added [35, 33] (but see [42] for an example in which the number of connections to a node is precisely conserved). The reason for doing this is to keep the balance of excitation and inhibition constant. If we were to add additional connections, for example, within the excititory population, the results seen might just be a result of increasing the number of connections, rather than their spatial arrangement. We are interested in the effects of rewiring connections from short range to long range, and thus use the form suggested in [45]. We replace (9)-(11) by

$$q_i = \frac{1}{N}\sum_{j=1}^{N} A_{ij}^{IE} P_n(\theta_j); \quad r_i = \frac{1}{N}\sum_{j=1}^{N} A_{ij}^{EE} P_n(\theta_j); \quad s_i = \frac{1}{N}\sum_{j=1}^{N} A_{ij}^{EI} P_n(\phi_j); \tag{15}$$

where

$$A_{ij}^{IE} = \begin{cases} 1 & \text{with probability } \begin{cases} 1-[1-(2M_{IE}+1)/N]p_1, & |i-j| \le M_{IE} \\ (2M_{IE}+1)p_1/N, & |i-j| > M_{IE} \end{cases} \\ 0 & \text{otherwise} \end{cases} \tag{16}$$

$$A_{ij}^{EE} = \begin{cases} 1 & \text{with probability } \begin{cases} 1-[1-(2M_{EE}+1)/N]p_2, & |i-j| \le M_{EE} \\ (2M_{EE}+1)p_2/N, & |i-j| > M_{EE} \end{cases} \\ 0 & \text{otherwise} \end{cases} \tag{17}$$

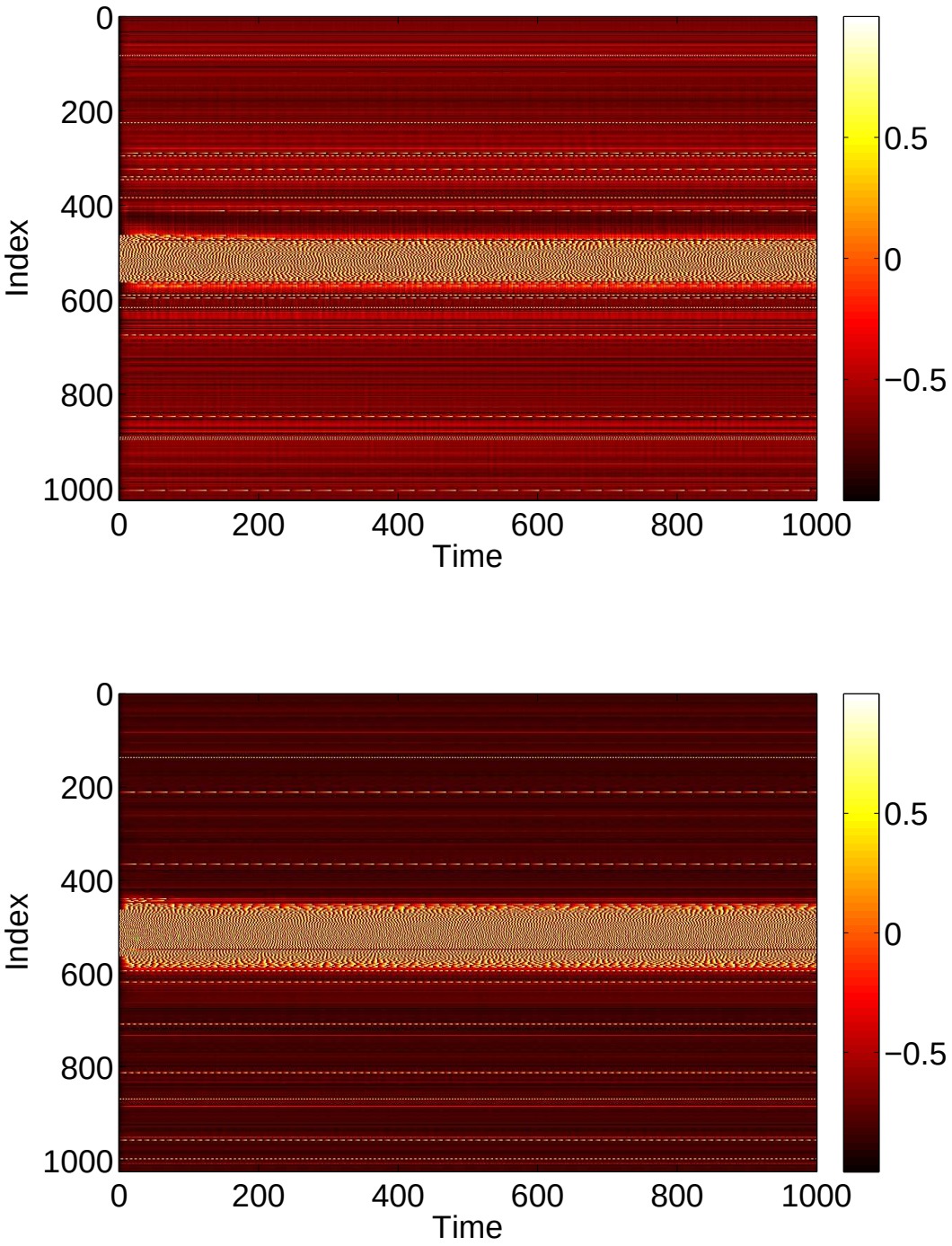

FIGURE 1. A bump solution of (3)-(6). Top: $\sin\theta_i$. Bottom: $\sin\phi_i$. Parameter values: $N = 1024, \Delta = 0.02, I_0 = -0.16, J_0 = -0.4, n = 2, g_{EE} = 25, g_{IE} = 25, g_{EI} = 7.5, M_{IE} = 40, M_{EE} = 40, M_{EI} = 60$ and $\tau = 10$.

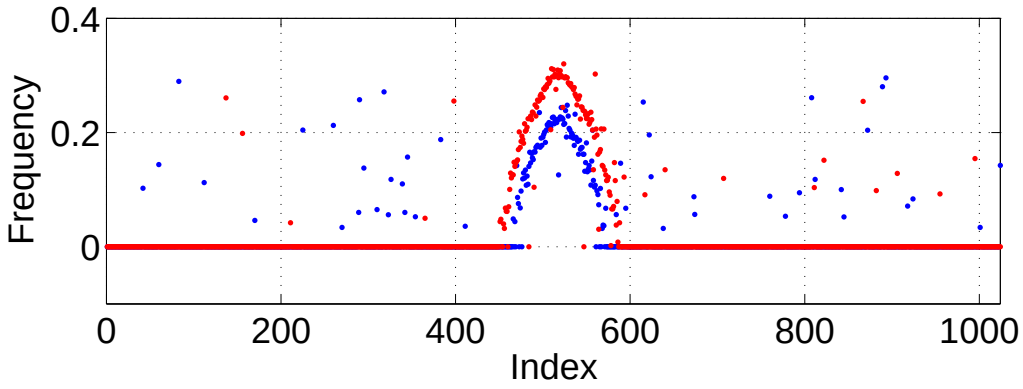

FIGURE 2. Average frequency for excitatory population (blue) and inhibitory (red) for the solution shown in Fig. 1.

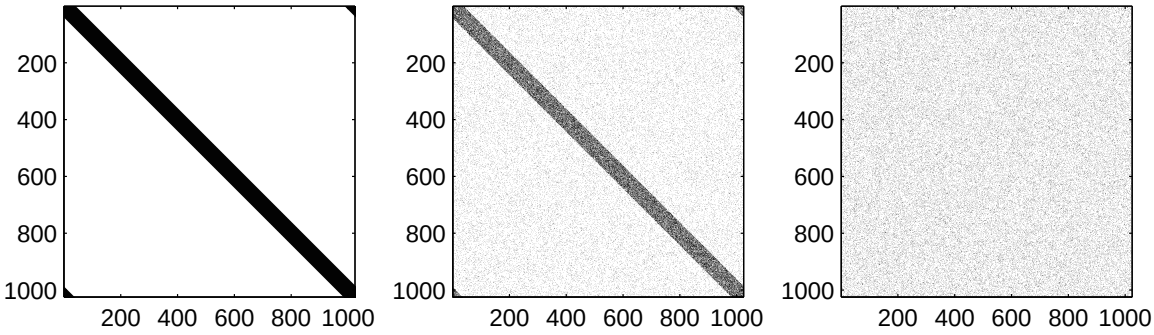

FIGURE 3. Typical realisations of A^{IE} for $p_1 = 0$ (left) 0.5 (middle) and 1 (right). $N = 1024, M_{IE} = 40$. Black corresponds to a matrix entry of 1, white to 0.

and

$$A_{ij}^{EI} = \begin{cases} 1 & \text{with probability } \begin{cases} 1-[1-(2M_{EI}+1)/N]p_3, & |i-j| \le M_{EI} \\ (2M_{EI}+1)p_3/N, & |i-j| > M_{EI} \end{cases} \\ 0 & \text{otherwise} \end{cases} \tag{18}$$

where $|i-j|$ refers to the shortest distance between neurons i and j, measured on the ring. When $p_1 = p_2 = p_3 = 0$, (15) reverts to (9)-(11). Note that when $p_1 = 1$, the probability of A_{ij}^{IE} being 1 is independent of i and j, and that the expected number of nonzero entries in a row of A_{ij}^{IE} (i.e. the expected number of connections from the excitatory population to an inhibitory neuron) is independent of p_1. Similar statements apply for the other two matrices and their parameters p_2 and p_3. Typical variation of A^{IE} with p_1 is shown in Fig. 3 and it is clear that increasing p_1 interpolates between purely local connections ($p_1 = 0$) and uniform random connectivity ($p_1 = 1$).

We could simply simulate (3)-(6) with (15) for particular values of p_1, p_2 and p_3 but we would like to gain a deeper understanding of the dynamics of such a network. The first approach is to take the continuum limit in which the number of neurons in each network goes to infinity, in a particular way.

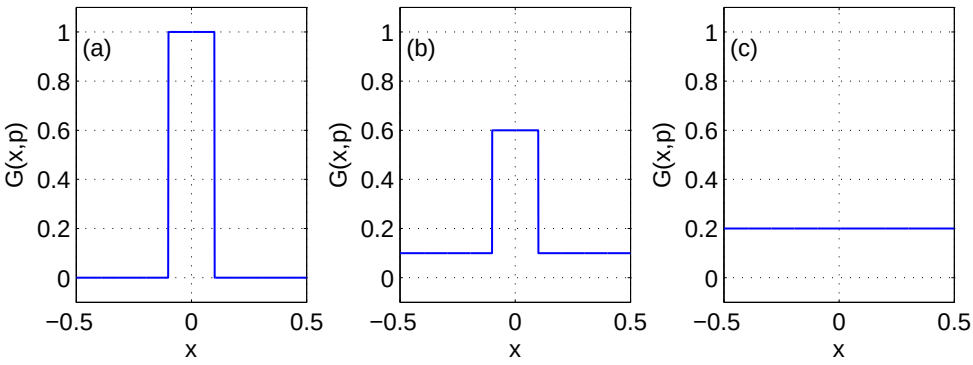

FIGURE 4. One of the functions (19)-(21) with (a): $p = 0$, (b): $p = 0.5$, and (c): $p = 1$. For this example, $\alpha = 0.1$. Note the similarity with the middle row of the matrices shown in Fig. 3.

2.3. **Continuum limit.** We take the continuum limit: $N, M_{EI}, M_{EE}, M_{IE} \to \infty$ such that $M_{EI}/N \to \alpha_{EI}$, $M_{EE}/N \to \alpha_{EE}$ and $M_{IE}/N \to \alpha_{IE}$, where $0 < \alpha_{EI}, \alpha_{EE}, \alpha_{IE} < 1/2$, and set the circumference of the ring of neurons to be 1. In this limit the sums (15) are replaced by integrals (more specifically, convolutions) with the connectivity kernels

$$G_{IE}(x,p_1) = \begin{cases} 1-(1-2\alpha_{IE})p_1, & |x| < \alpha_{IE} \\ 2\alpha_{IE}p_1, & \text{otherwise} \end{cases} \tag{19}$$

$$G_{EE}(x,p_2) = \begin{cases} 1-(1-2\alpha_{EE})p_2, & |x| < \alpha_{EE} \\ 2\alpha_{EE}p_2, & \text{otherwise} \end{cases} \tag{20}$$

$$G_{EI}(x,p_3) = \begin{cases} 1-(1-2\alpha_{EI})p_3, & |x| < \alpha_{EI} \\ 2\alpha_{EI}p_3, & \text{otherwise} \end{cases} \tag{21}$$

where $G_{IE}(x,p_1)$ is the probability that a point in the excitatory population is connected to a point in the inhibitory population a distance x away, and similarly for the other two kernels. The effect of varying $p_j, j = 1,2,3$, on one of the functions (19)-(21) is shown in Fig. 4. Taking G_{IE} for example, we see that $\int_{-1/2}^{1/2} G_{IE}(x,p_1)\,dx = 2\alpha_{IE}$ independent of p_1, i.e. the expected total number of connections is preserved, and similarly for the other two functions.

Taking the continuum limit of (3)-(6) we describe the dynamics of the θ_i and ϕ_i in terms of probability densities $F_E(\theta,x,I,t)$ and $F_I(\phi,x,J,t)$, respectively, where x and t are (continuous) space and time, and I and J are random variables with densities $h(I)$ and $g(J)$ respectively. F_E satisfies the continuity equation [31]

$$\frac{\partial F_E}{\partial t} + \frac{\partial}{\partial \theta}\left\{F_E\left[1-\cos\theta + (1+\cos\theta)(I + g_{EE}v - g_{EI}s)\right]\right\} = 0 \tag{22}$$

and similarly F_I satisfies

$$\frac{\partial F_I}{\partial t} + \frac{\partial}{\partial \phi}\left\{F_I\left[1-\cos\phi + (1+\cos\phi)(J + g_{IE}u)\right]\right\} = 0 \tag{23}$$

where

$$\tau\frac{\partial v}{\partial t}=r-v \tag{24}$$

$$\tau\frac{\partial u}{\partial t}=q-u \tag{25}$$

and

$$q(x,t)=\int_0^1 G_{IE}(|x-y|,p_1)\int_{-\infty}^{\infty}\int_0^{2\pi}F_E(\theta,y,I,t)a_n(1-\cos\theta)^n d\theta\ dI\ dy \tag{26}$$

$$r(x,t)=\int_0^1 G_{EE}(|x-y|,p_2)\int_{-\infty}^{\infty}\int_0^{2\pi}F_E(\theta,y,I,t)a_n(1-\cos\theta)^n d\theta\ dI\ dy \tag{27}$$

$$s(x,t)=\int_0^1 G_{EI}(|x-y|,p_3)\int_{-\infty}^{\infty}\int_0^{2\pi}F_I(\phi,y,J,t)a_n(1-\cos\phi)^n d\phi\ dJ\ dy \tag{28}$$

The forms of (22) and (23) mean that they are amenable to the use of the Ott/Antonsen ansatz [36, 37]. This ansatz states that if the neurons are not identical (i.e. $\Delta > 0$ for the networks studied here), solutions of the continuity equations (22) and (23) decay exponentially onto a lower-dimensional manifold on which the θ and ϕ dependence of F_E and F_I, respectively, have a particular form. This form is a Fourier series in θ (or ϕ) in which the nth coefficient is some function to the nth power. (See (57), for example.) Thus we can restrict (22) and (23) to this manifold, thereby simplifying the dynamics.

The standard Kuramoto order parameter for an all-to-all coupled network with phases $\{\theta_j\}$ is the expected value of $e^{i\theta_j}$ [46]. For the network studied here we can define the analogous spatially-dependent order parameters for the excitatory and inhibitory networks as

$$z_E(x,t)=\int_{-\infty}^{\infty}\int_0^{2\pi}F_E(\theta,x,I,t)e^{i\theta}\ d\theta\ dI \tag{29}$$

and

$$z_I(x,t)=\int_{-\infty}^{\infty}\int_0^{2\pi}F_I(\phi,x,J,t)e^{i\phi}\ d\phi\ dJ \tag{30}$$

respectively. For fixed x and t, $z_E(x,t)$ is a complex number with a phase and a magnitude. The phase gives the most likely value of θ and the magnitude governs the "sharpness" of the probability distribution of θ (at that x and t), and similarly for $z_I(x,t)$ and ϕ [22, 24]. We can also determine from z_E and z_I the instantaneous firing rate of each population (see Sec. 3.1 and [34]).

Performing manipulations as in [22, 24, 31, 44] we obtain the continuum limit of (3)-(6): evolution equations for z_E and z_I

$$\frac{\partial z_E}{\partial t}=\frac{(iI_0-\Delta)(1+z_E)^2-i(1-z_E)^2}{2}+\frac{i(1+z_E)^2(g_{EE}v-g_{EI}s)}{2} \tag{31}$$

$$\frac{\partial z_I}{\partial t}=\frac{(iJ_0-\Delta)(1+z_I)^2-i(1-z_I)^2}{2}+\frac{i(1+z_I)^2 g_{IE}u}{2} \tag{32}$$

together with (24)-(25), where

$$q(x,t) = \int_0^1 G_{IE}(|x-y|,p_1)H(z_E(y,t);n)dy \tag{33}$$

$$r(x,t) = \int_0^1 G_{EE}(|x-y|,p_2)H(z_E(y,t);n)dy \tag{34}$$

$$s(x,t) = \int_0^1 G_{EI}(|x-y|,p_3)H(z_I(y,t);n)dy \tag{35}$$

and

$$H(z;n) = a_n\left[C_0 + \sum_{q=1}^{n} C_q\left(z^q + \bar{z}^q\right)\right] \tag{36}$$

where

$$C_q = \sum_{k=0}^{n}\sum_{m=0}^{k} \frac{n!(-1)^k \delta_{k-2m,q}}{2^k(n-k)!m!(k-m)!} \tag{37}$$

and where by $|x-y|$ in (26)-(28) we mean the shortest distance between x and y given that they are both points on a circle, i.e. $|x-y| = \min\left(|x-y|, 1-|x-y|\right)$.

The advantage of this continuum formulation is that bumps like that in Fig. 1 are fixed points of (31)-(32) and (24)-(25). Once these equations have been spatially discretised, we can find fixed points of them using Newton's method, and determine the stability of these fixed points by finding the eigenvalues of the linearisation around them. We can also follow these fixed points as parameter are varied, detecting (local) bifurcations [23]. The results of varying p_1, p_2 and p_3 independently are shown in Sec. 3.1.

2.4. **Infinite ensembles.** We now consider the case where N is fixed and finite, and so are the matrices A^{IE}, A^{EE} and A^{EI}, but we average over an infinite ensemble of networks with these connectivities, where each member of the ensemble has a different (but consistent) realisation of the random currents I_i and J_i [5, 28]. This procedure results in $4N$ ordinary differential equations (ODEs), $2N$ of them for complex quantities and the other $2N$ for real quantities. Thus there is no reduction of dimension from the original system (3)-(6), but as in Sec. 2.3, bump states will be fixed points of these ODEs.

Letting the number of members in the ensemble go to infinity, we describe the state of the excitatory network by the probability density function

$$f^E(\theta_1,\theta_2,\ldots,\theta_N;I_1,I_2,\ldots I_N;t) \equiv f^E(\{\theta\};\{I\};t) \tag{38}$$

and that of the inhibitory one by

$$f^I(\phi_1,\phi_2,\ldots,\phi_N;J_1,J_2,\ldots J_N;t) \equiv f^I\left(\{\phi\};\{J\};t\right) \tag{39}$$

which satisfy the continuity equations

$$\frac{\partial f^E}{\partial t} + \sum_{j=1}^{N}\frac{\partial}{\partial\theta_j}\left[f^E\left(\frac{d\theta_j}{dt}\right)\right] = 0 \tag{40}$$

and

$$\frac{\partial f^I}{\partial t} + \sum_{j=1}^{N}\frac{\partial}{\partial\phi_j}\left[f^I\left(\frac{d\phi_j}{dt}\right)\right] = 0 \tag{41}$$

where $d\theta_j/dt$ and $d\phi_j/dt$ are given by (3) and (4).

Performing the manipulations in Appendix A we obtain

$$\frac{dz_j^E}{dt} = \frac{(iI_0-\Delta)\left(1+z_j^E\right)^2 - i\left(1-z_j^E\right)^2}{2} + \frac{i(1+z_j^E)^2(g_{EE}v_j - g_{EI}s_j)}{2} \tag{42}$$

$$\frac{dz_j^I}{dt} = \frac{(iJ_0-\Delta)\left(1+z_j^I\right)^2 - i\left(1-z_j^I\right)^2}{2} + \frac{i\left(1+z_j^I\right)^2 g_{IE}u_j}{2} \tag{43}$$

for $j = 1, 2, \ldots N$ where

$$q_i = \frac{1}{N}\sum_{j=1}^{N} A_{ij}^{IE} H\left(z_j^E(t); n\right) \tag{44}$$

$$r_i = \frac{1}{N}\sum_{j=1}^{N} A_{ij}^{EE} H\left(z_j^E(t); n\right) \tag{45}$$

$$s_i = \frac{1}{N}\sum_{j=1}^{N} A_{ij}^{EI} H\left(z_j^I(t); n\right) \tag{46}$$

and

$$\tau\frac{dv_i}{dt} = r_i - v_i \tag{47}$$

$$\tau\frac{du_i}{dt} = q_i - u_i \tag{48}$$

for $i = 1, 2, \ldots N$. Equations (42)-(48) form a complete description of the *expected* behaviour of a network with connectivities given by the matrices A^{IE}, A^{EE} and A^{EI}. Note the similarities with (31)-(35) and (24)-(25). As mentioned above, the advantage of this formulation is that states like that in Fig. 1 will be fixed points of (42)-(48), for the specified connectivities.

Recalling that the matrices A^{IE}, A^{EE} and A^{EI} depend on the parameters p_1, p_2 and p_3 respectively we now investigate how solutions of (42)-(48) depend on these parameters. One difficulty in trying to vary, say, p_1, is that the entries of A^{IE} do not depend continuously on p_1. Indeed, as presented, one should recalculate A^{IE} each time p_1 is changed. In order to generate results comparable with those from Sec. 2.3 we introduce a consistent family of matrices, following [33]. Consider A^{IE} (similar procedures apply for the other two matrices) and define an $N \times N$ matrix r, each entry of which is independently and randomly chosen from a uniform distribution on the interval $(0, 1)$. The matrix r is now considered to be fixed, and we define $A^{IE}(p_1)$ as follows:

$$A_{ij}^{IE}(p_1) = \begin{cases} \Theta[r_{ij} - p_1(1-(2M_{IE}+1)/N)], & |i-j| \le M_{IE} \\ \Theta[r_{ij} - (1-p_1(2M_{IE}+1)/N)], & |i-j| > M_{IE} \end{cases} \tag{49}$$

where Θ is the Heaviside step function and the indices are taken modulo N. Comparing this with (16) we see that for a fixed p_1, generating a new r and using (49) is equivalent to generating A^{IE} using (16). The reason for using (49) is that since the r_{ij} are chosen once and then fixed, an entry in A^{IE} will switch from 0 to 1 (or vice versa) at most once as p_1 is varied monotonically in the interval $[0, 1]$.

The effects of quasistatically increasing p_1 and p_3 for (42)-(48) are shown in Sec. 3.2.

3. Results

3.1. **Results for continuum limit.** For the system (31)-(32) and (24)-(25) we discretise the spatial domain into 1024 evenly spaced points and approximate the integrals in (33)-(35) with Riemann sums. We numerically integrate the spatially-discretised evolution equations in time, using appropriate initial conditions, until a steady state is reached. This steady state is then continued using pseudo-arclength continuation, and the stability of the solutions found determined by examining the eigenvalues of the Jacobian evaluated at them [23]. The increment between successive values of the p_i found during continuation is not fixed and the numerical results found were interpolated to a uniform grid for plotting in Figs. 5, 7 and 8. We consider varying p_1, p_2 and p_3 independently, keeping the other two parameters fixed at zero. The results of varying p_1 are shown in Fig. 5, where we plot the firing rate of the two populations, derived as $\mathrm{Re}(w_i)/\pi$ where $w_i = (1-\bar{z}_i)/(1+\bar{z}_i)$ for $i = I, E$, as in [34], where the z_i are fixed points of (31)-(32). We see an increase and then decrease in bump width as p_1 is increased. There is also a pair of supercritical Hopf bifurcations, between which the bump is unstable. (It is only weakly unstable, with the rightmost eigenvalue of the Jacobian having a maximal real part of 0.015 in this interval.) At the leftmost Hopf bifurcation the Jacobian has eigenvalues $\pm 1.8191i$ and at the rightmost it has eigenvalues $\pm 1.7972i$, with all other eigenvalues having negative real parts. One notable aspect is the increase in firing rate of the inhibitory population "outside" the bump as p_1 is increased, such that when $p_1 = 1$ the firing rate in this population is spatially homogeneous. This is to be expected, as there are no inhibitory-to-inhibitory connections, and when $p_1 = 1$ all inhibitory neurons receive the same input from the excitatory population.

Increasing p_2 while keeping $p_1 = p_3 = 0$ we find that the bump undergoes a Hopf bifurcation (Jacobian has eigenvalues $\pm 0.3404i$) and then is destroyed in a saddle-node bifurcation at $p_2 \approx 0.48$, as shown in Fig. 6. The behaviour of the bumps for $0 \leq p_2 \leq 0.48$ is shown in Fig. 7.

Varying p_3 we obtain Fig. 8, where there are no bifurcations as p_3 is increased all the way to 1, corresponding to the case where all excitatory neurons feel the same inhibition, just a weighted mean of the output from the inhibitory population. We again see an increase and then slight decrease in bump width as p_3 is increased.

While a Hopf bifurcation of a bump may seem undesirable from a neurocomputational point of view, it should be kept in mind that oscillations are an essential phenomenon in many different neural networks, and they are widely studied [4].

We have only varied one of p_1, p_2 and p_3, keeping the other two probabilities at zero. A clearer picture of the system's behaviour could be obtained by simultaneously varying two, or all three, of these probabilities. We leave this as future work, but mention that for the special case $p_1 = p_2 = p_3 = p$, the bump persists and is stable up to $p \approx 0.49$, where it undergoes a saddle-node bifurcation (not shown).

3.2. **Results for infinite ensemble.** This section refers to equations (42)-(48). In Fig. 9 we show the results of slowly increasing p_1, while keeping $p_2 = p_3 = 0$. We initially set $p_1 = 0$ and integrated (42)-(48) to a steady state, using initial conditions that give a bump solution. We then increased p_1 by 0.01 and integrated (42)-(48) again for 10,000 time units, using as an initial condition the final state of the previous integration. We continued this process up to $p_1 = 1$. The firing rate for the jth excitatory neuron is $\mathrm{Re}(w_j)/\pi$ where $w_j = (1-\bar{z}_j^E)/(1+\bar{z}_j^E)$, and similarly for an inhibitory neuron. Comparing Fig. 9 with Fig. 5 we see the same behaviour, the main difference being that the bump now moves in an unpredictable way around the domain as p_1 is increased. This is due to the system no longer being translationally invariant, and the bump moving to a position in which it is stable [47]. Unlike

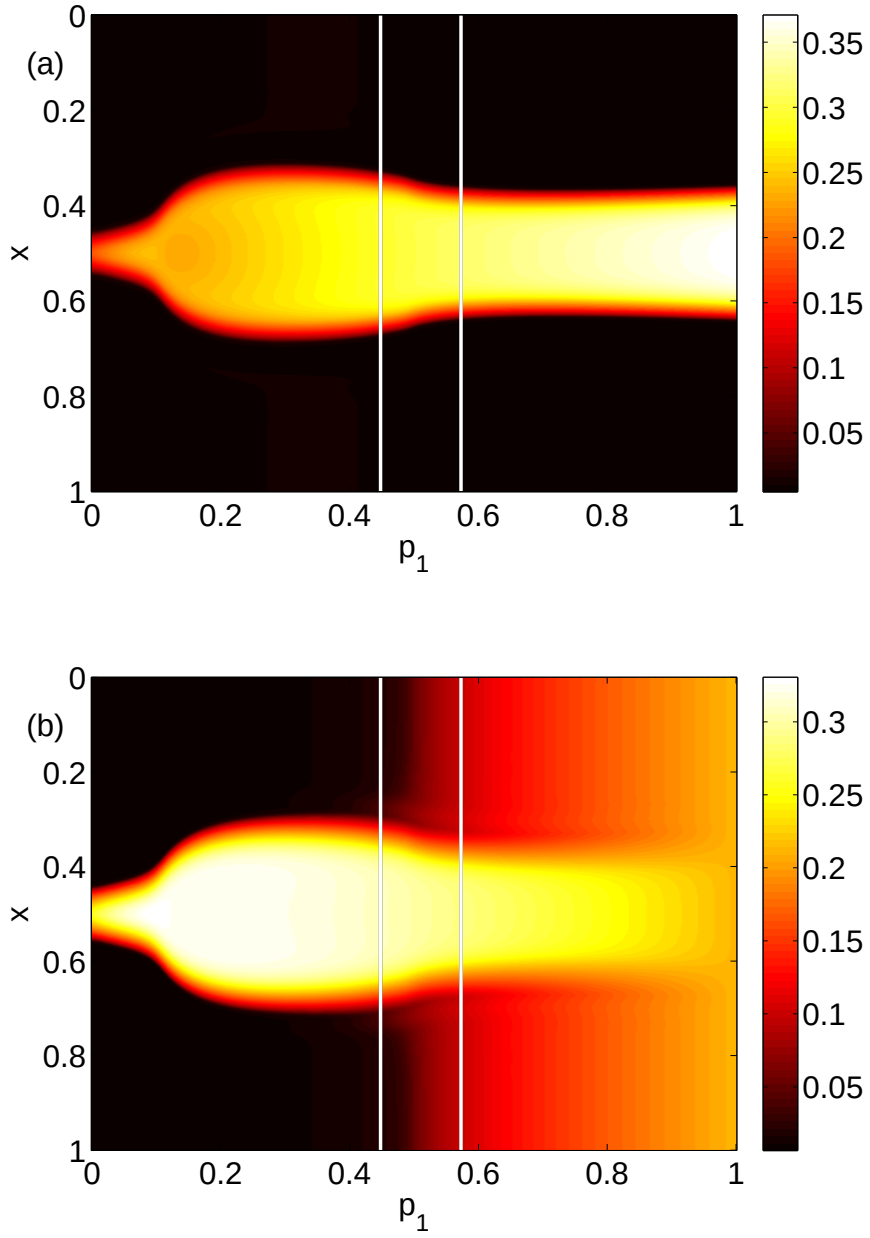

FIGURE 5. Firing rate for (a): excitatory population and (b): inhibitory population, as a function of p_1, with $p_2 = p_3 = 0$. There is a Hopf bifurcation on both white vertical lines and the bump is unstable between these. Other parameters: $\Delta = 0.02, I_0 = -0.16, J_0 = -0.4, n = 2, g_{EE} = 25$, $g_{IE} = 25, g_{EI} = 7.5, \alpha_{IE} = 40/1024, \alpha_{EE} = 40/1024, \alpha_{EI} = 60/1024$ and $\tau = 10$.

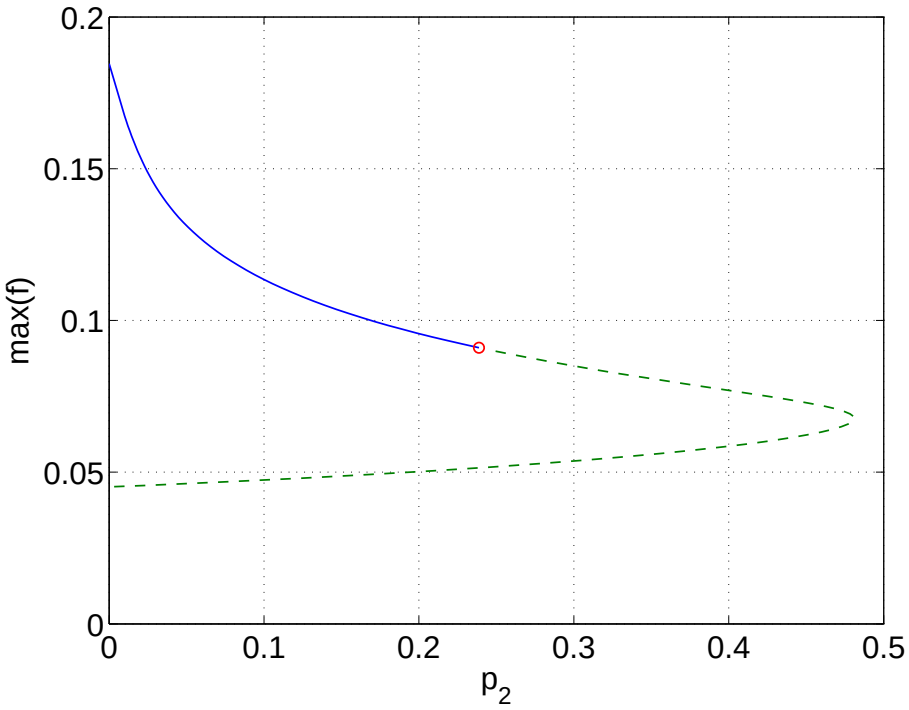

FIGURE 6. Maximum (over x) of the firing rate for the excitatory population as a function of p_2 with $p_1 = p_3 = 0$. Solid: stable; dashed: unstable. The Hopf bifurcation is marked with a circle. Other parameters: $\Delta = 0.02, I_0 = -0.16, J_0 = -0.4, n = 2, g_{EE} = 25$, $g_{IE} = 25, g_{EI} = 7.5, \alpha_{IE} = 40/1024, \alpha_{EE} = 40/1024, \alpha_{EI} = 60/1024$ and $\tau = 10$.

the situation shown in Fig. 5 we did not observe any Hopf bifurcations, for this realisation of the A^{IE}. Presumably this is also a result of breaking the translational invariance and the weakly unstable nature of the bump shown in Fig. 5 between the Hopf bifurcations.

Repeating this process as p_3 is varied with $p_1 = p_2 = 0$ we obtain the results in Fig. 10. Comparing with Fig. 8 we see very good agreement, although the bump does move considerably for small p_3, as in Fig. 9. Varing p_2 with $p_1 = p_3 = 0$ we obtain similar results to those in Fig. 7 (not shown). Typical behaviour of (42)-(48) with $p_2 = 0.3$ (i.e. beyond the Hopf bifurcation shown in Fig. 7) is shown in Fig. 11, where the oscillations are clearly seen.

3.3. **Results for original network.** To verify the results obtained above we ran the full network (3)-(6) but using the connectivity (49) (and similar constructions for A^{EE} and A^{EI}) to calculate (15). The frequency was measured directly from simulations. Varying p_1 we obtain the results in Fig. 12; again, no oscillatory behaviour associated with a Hopf bifurcation was observed and the results are similar to those in Fig. 9. Varying p_3 we obtained Fig. 13 (compare with Fig. 10). Fig. 14 shows oscillatory behaviour at $p_2 = 0.3, p_1 = p_3 = 0$ (the same parameter values as used in Fig. 11).

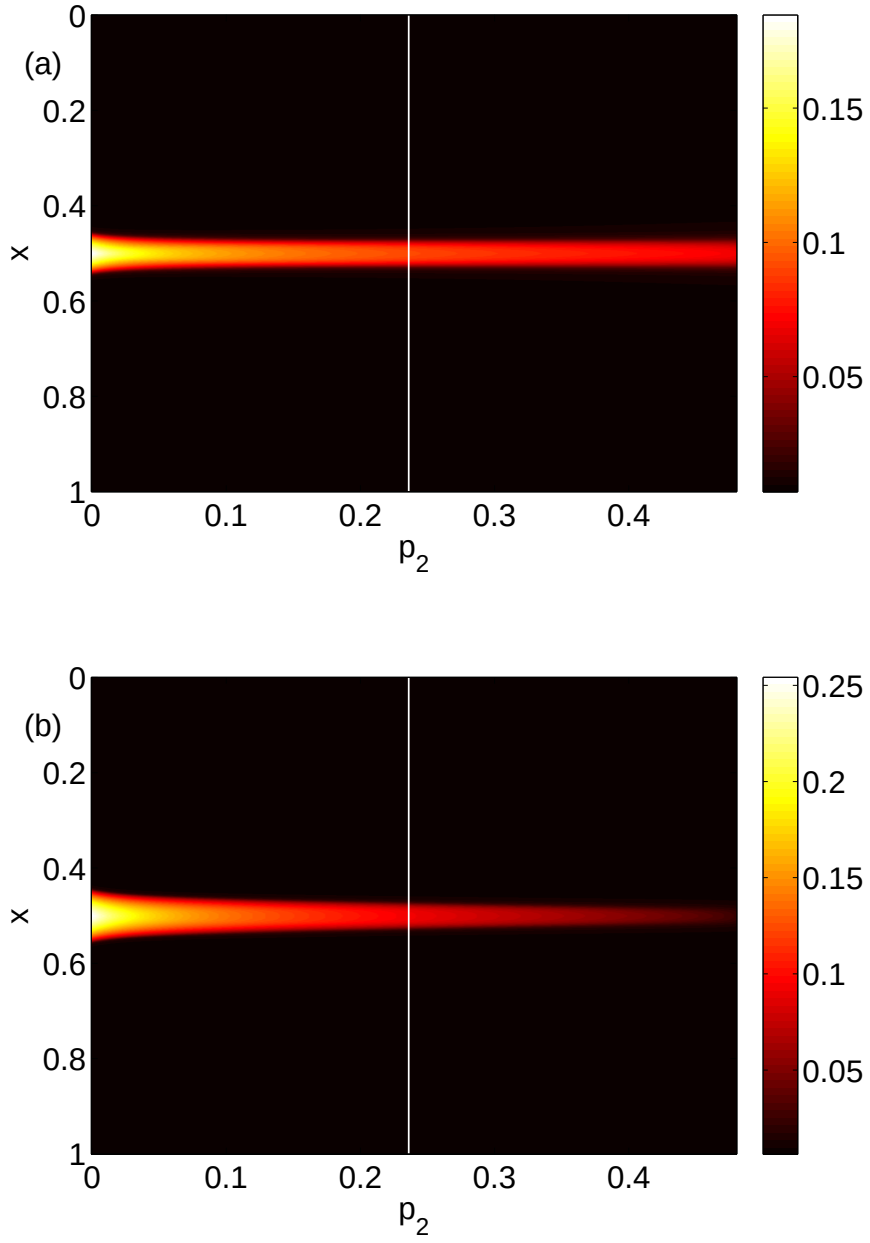

FIGURE 7. Firing rate for (a): excitatory population and (b): inhibitory population, as a function of p_2, with $p_3 = p_1 = 0$. There is a Hopf bifurcation at the white vertical line and the bump is destroyed in saddle-node bifurcation at $p_2 \approx 0.48$. Other parameters: $\Delta = 0.02, I_0 = -0.16, J_0 = -0.4, n = 2, g_{EE} = 25$, $g_{IE} = 25, g_{EI} = 7.5, \alpha_{IE} = 40/1024, \alpha_{EE} = 40/1024, \alpha_{EI} = 60/1024$ and $\tau = 10$.

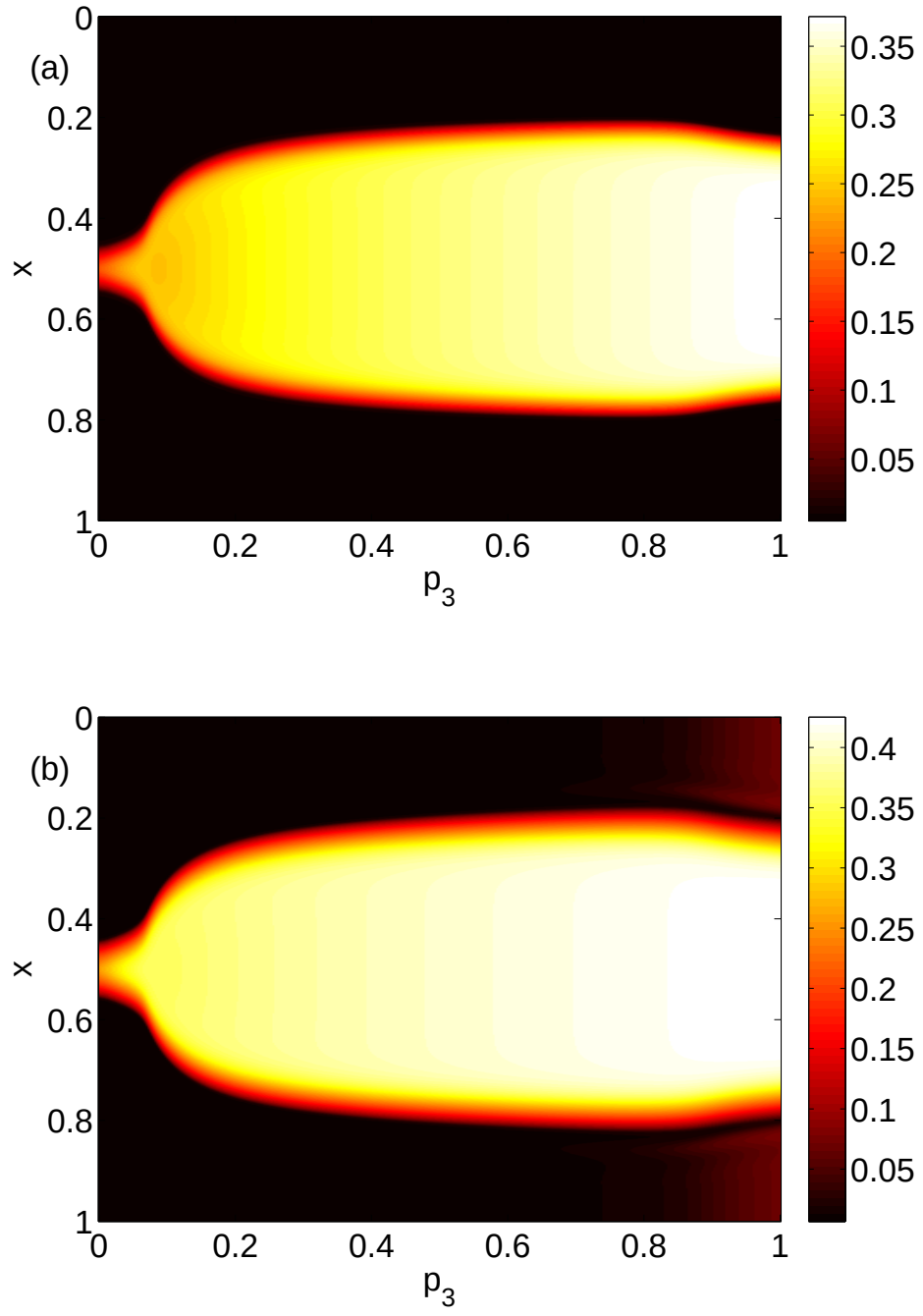

FIGURE 8. Firing rate for (a): excitatory population and (b): inhibitory population, as a function of p_3, with $p_2 = p_1 = 0$. Other parameters: $\Delta = 0.02, I_0 = -0.16, J_0 = -0.4, n = 2, g_{EE} = 25,\ g_{IE} = 25, g_{EI} = 7.5, \alpha_{IE} = 40/1024, \alpha_{EE} = 40/1024, \alpha_{EI} = 60/1024$ and $\tau = 10$.

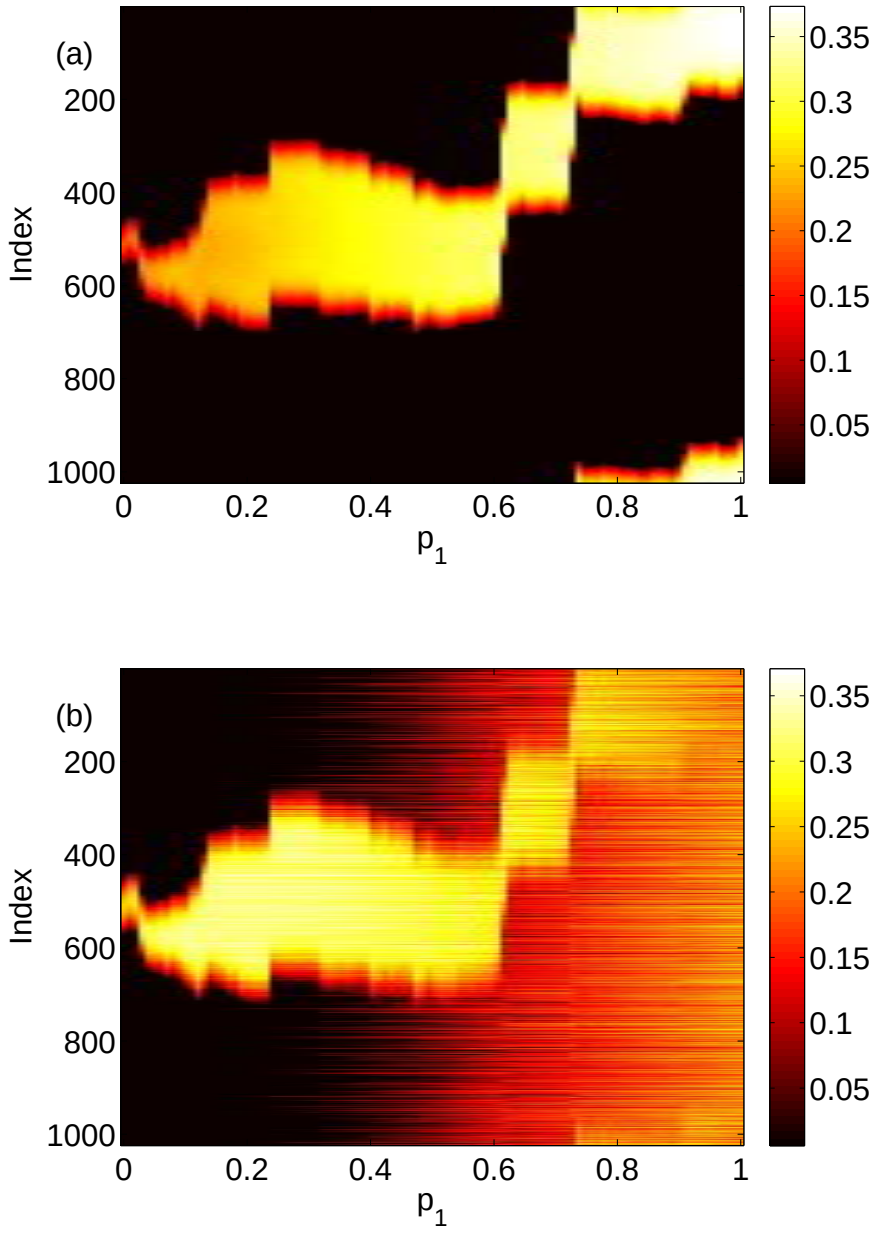

FIGURE 9. Firing rate for (a): excitatory population and (b): inhibitory population, as a function of p_1, with $p_2 = p_3 = 0$. Compare with Fig. 5. Other parameters: $\Delta = 0.02, I_0 = -0.16, J_0 = -0.4, n = 2, g_{EE} = 25$, $g_{IE} = 25, g_{EI} = 7.5, N = 1024, M_{IE} = 40, M_{EE} = 40, M_{EI} = 60$ and $\tau = 10$.

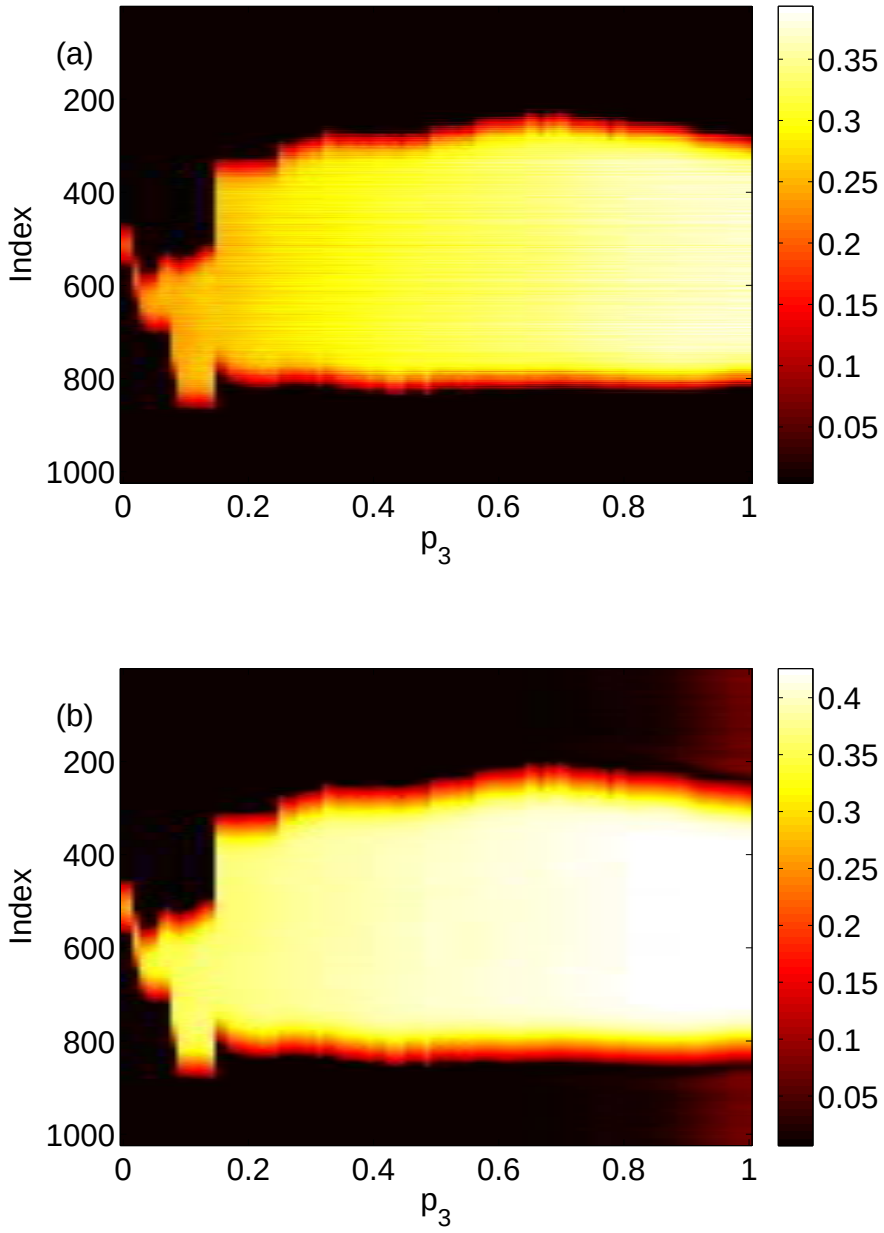

FIGURE 10. Firing rate for (a): excitatory population and (b): inhibitory population, as a function of p_3, with $p_2 = p_1 = 0$. Compare with Fig. 8. Other parameters: $\Delta = 0.02, I_0 = -0.16, J_0 = -0.4, n = 2, g_{EE} = 25,\ g_{IE} = 25, g_{EI} = 7.5, N = 1024, M_{IE} = 40, M_{EE} = 40, M_{EI} = 60$ and $\tau = 10$.

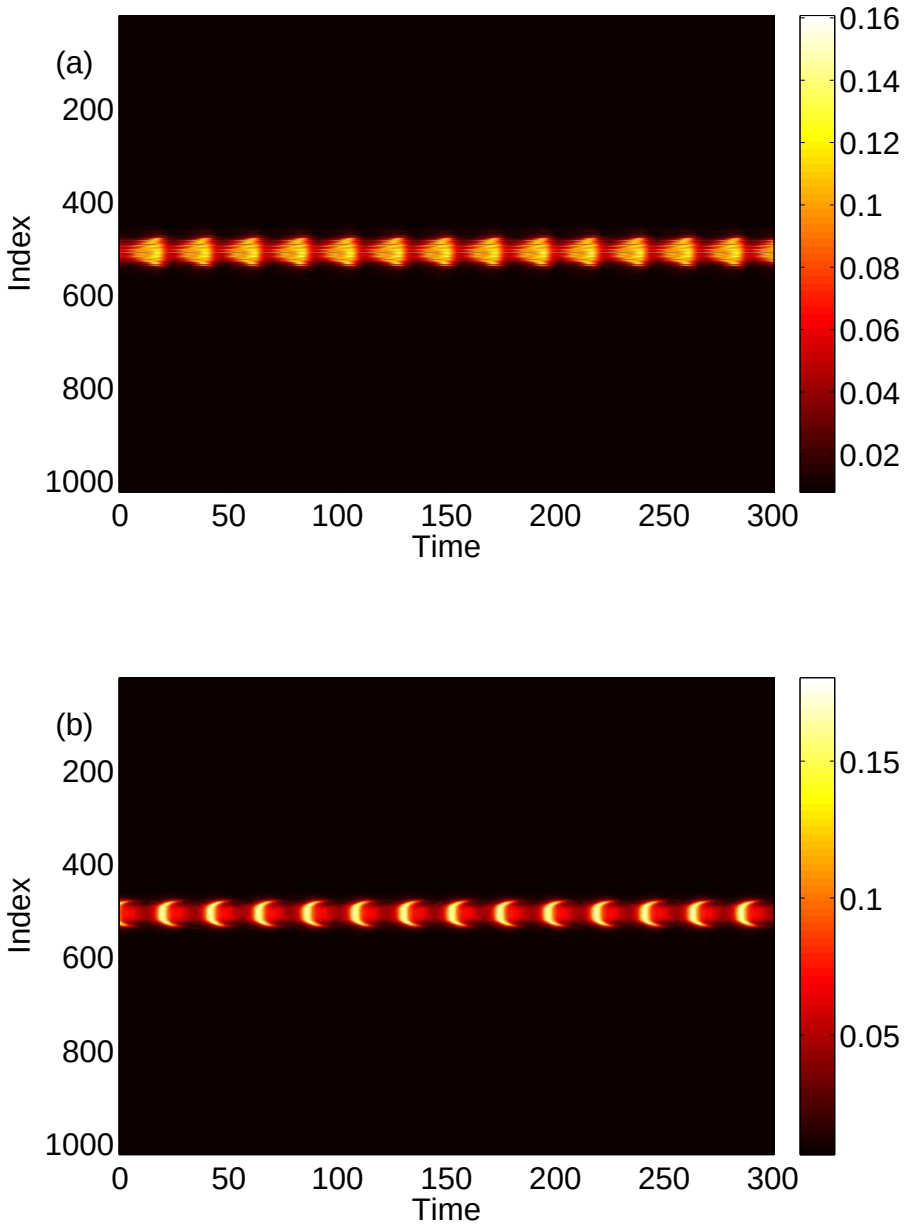

FIGURE 11. Instantaneous firing rate for (a): excitatory population and (b): inhibitory population, with $p_2 = 0.3$ and $p_3 = p_1 = 0$. Other parameters: $\Delta = 0.02, I_0 = -0.16, J_0 = -0.4, n = 2, g_{EE} = 25$, $g_{IE} = 25, g_{EI} = 7.5, N = 1024, M_{IE} = 40, M_{EE} = 40, M_{EI} = 60$ and $\tau = 10$.

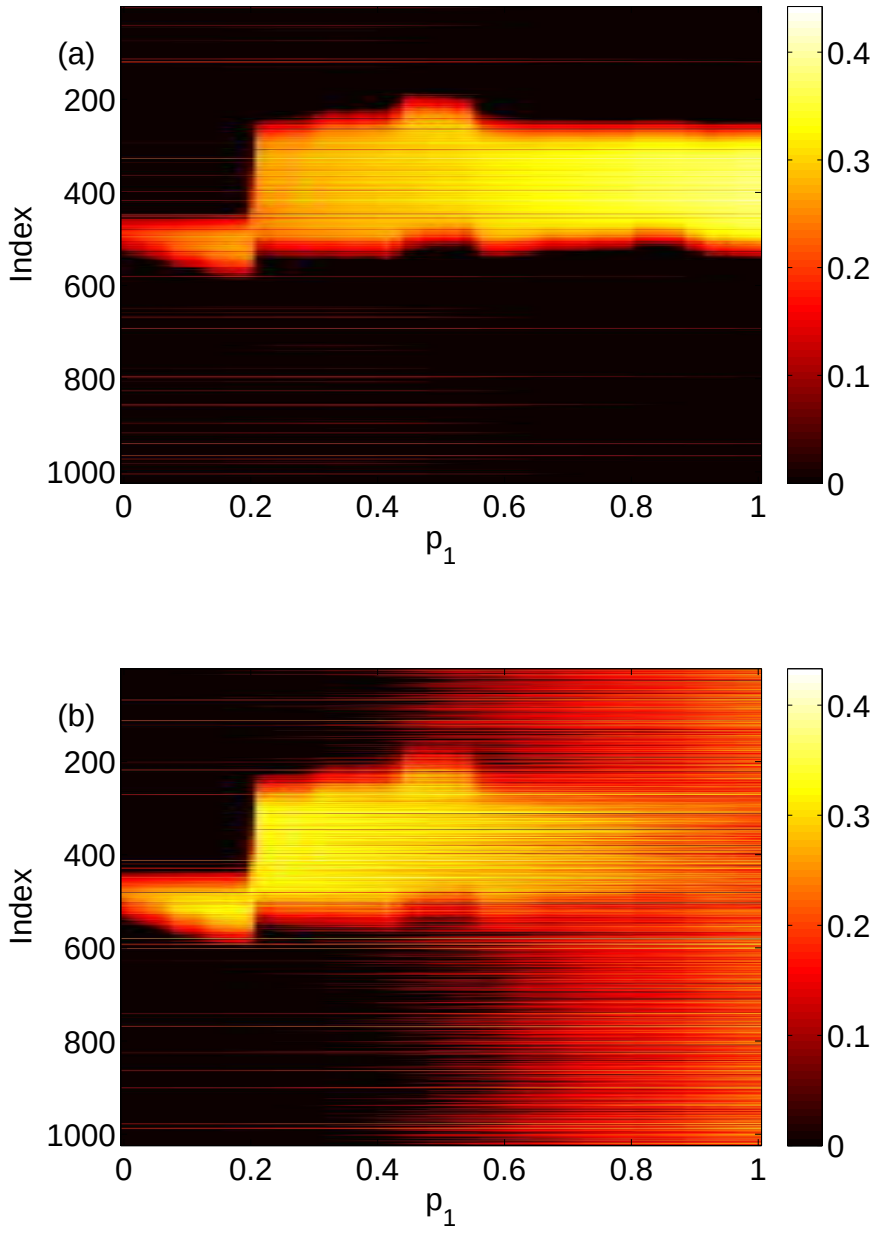

FIGURE 12. Firing rate for (a): excitatory population and (b): inhibitory population in the full network (3)-(6), averaged over a time window of length 500, as a function of p_1 with $p_2 = p_3 = 0$. Compare with Fig. 9. Other parameters: $\Delta = 0.02, I_0 = -0.16, J_0 = -0.4, n = 2, g_{EE} = 25$, $g_{IE} = 25, g_{EI} = 7.5, N = 1024, M_{IE} = 40, M_{EE} = 40, M_{EI} = 60$ and $\tau = 10$.

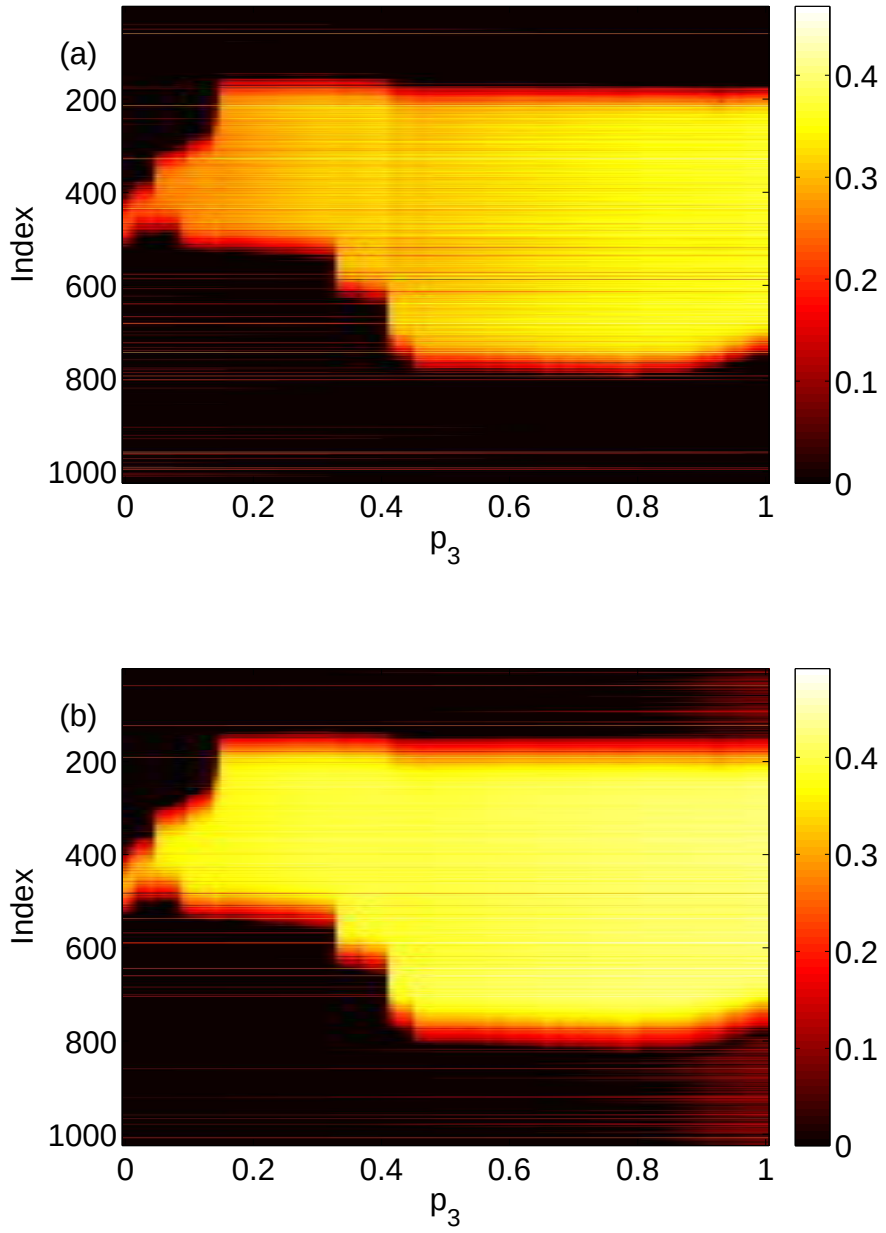

FIGURE 13. Firing rate for (a): excitatory population and (b): inhibitory population in the full network (3)-(6), averaged over a time window of length 500, as a function of p_3 with $p_2 = p_1 = 0$. Compare with Fig. 10. Other parameters: $\Delta = 0.02, I_0 = -0.16, J_0 = -0.4, n = 2, g_{EE} = 25$, $g_{IE} = 25, g_{EI} = 7.5, N = 1024, M_{IE} = 40, M_{EE} = 40, M_{EI} = 60$ and $\tau = 10$.

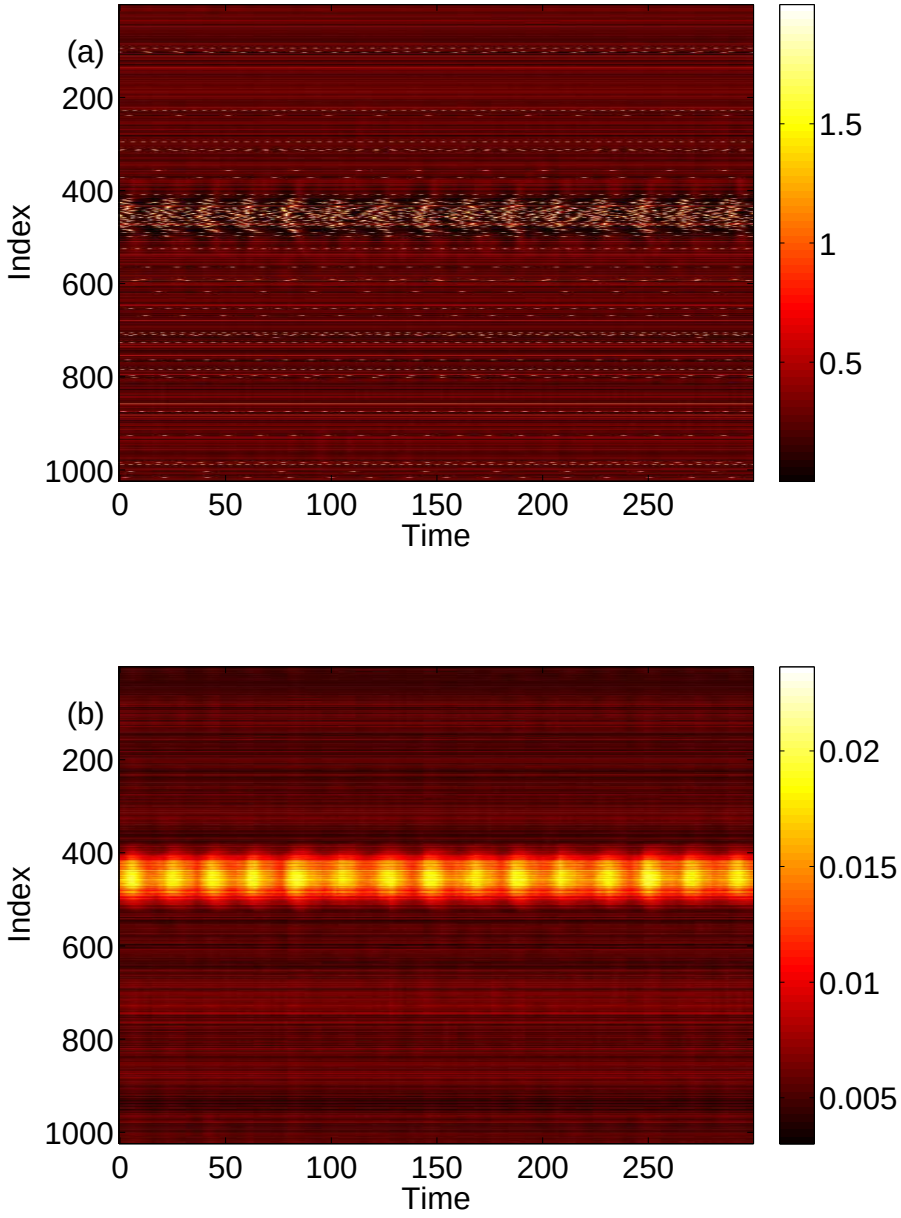

FIGURE 14. Behaviour of the full network (3)-(6) with $p_2 = 0.3$ and $p_3 = p_1 = 0$. (a): $1 - \cos\theta_j$, (b): v_j. Compare with Fig. 11. Other parameters: $\Delta = 0.02, I_0 = -0.16, J_0 = -0.4, n = 2, g_{EE} = 25$, $g_{IE} = 25, g_{EI} = 7.5, N = 1024, M_{IE} = 40, M_{EE} = 40, M_{EI} = 60$ and $\tau = 10$.

Note that the results in Figs. 9-14 are each for a single realisation of a typical (parametrised) small-world network. To gain insight into general small-world networks it would be of interest to study the statistics of the behaviour of such networks.

4. Discussion

We have considered the effects of randomly adding long-range and simultaneously removing short-range connections in a network of model theta neurons which is capable of supporting spatially localised bump solutions. Such rewiring makes the networks small-world, at least for small values of the rewiring probabilities. By using theta neurons we are able to use the Ott/Antonsen ansatz to derive descriptions of the networks in two limits: an infinite number of neurons, and an infinite ensemble of finite networks, each with the same connectivity. The usefulness of this is that the bumps of interest are *fixed points* of the dynamical equations derived in these ways, and can thus be found, their stability determined, and followed as parameters are varied using standard dynamical systems techniques.

For the parameters chosen we found bumps to be surprisingly robust: in several cases a rewiring probability could be taken from 0 to 1 without destroying a bump. However, rewiring connections within the excitatory population (increasing p_2) was found to destabilise a bump through a Hopf bifurcation and later destroy the unstable bump in a saddle-node bifurcation. Simulations of the full network were used to verify our results.

The network studied has many parameters: the spatial spread of local couplings, the timescale of excitatory synapses, the connection strengths within and between populations, and the distributions of heterogeneous input currents. These were all set so that the network without rewiring supported a stable bump solution, but we have not investigated the effects of varying any of these parameters. However, even without considering rewiring, equations (31)-(35) and (24)-(25) provide a framework for investigating the effects of varying these parameters on the existence and stability of bump solutions, since these continuum equations are derived directly from networks of spiking neurons, unlike many neural field models.

Acknowledgements: I thank the referees for their useful suggestions.

Appendix A. Mathematical details relating to Sec. 2.4

In the limit of an infinite ensemble we have

$$q_i = \frac{1}{N}\sum_{j=1}^{N} A_{ij}^{IE} \int\cdots\int P_n(\theta_j) f^E(\{\theta\};\{I\};t)\ d\theta_1\ d\theta_2 \ldots d\theta_N\ dI_1\ dI_2 \ldots dI_N$$
$$= \frac{1}{N}\sum_{j=1}^{N} A_{ij}^{IE} \int_{-\infty}^{\infty}\int_{0}^{2\pi} P_n(\theta_j) f_j^E(\theta_j, I_j, t) d\theta_j\ dI_j \tag{50}$$

$$r_i = \frac{1}{N}\sum_{j=1}^{N} A_{ij}^{EE} \int\cdots\int P_n(\theta_j) f^E(\{\theta\};\{I\};t)\ d\theta_1\ d\theta_2 \ldots d\theta_N\ dI_1\ dI_2 \ldots dI_N$$
$$= \frac{1}{N}\sum_{j=1}^{N} A_{ij}^{EE} \int_{-\infty}^{\infty}\int_{0}^{2\pi} P_n(\theta_j) f_j^E(\theta_j, I_j, t) d\theta_j\ dI_j \tag{51}$$

$$s_i = \frac{1}{N}\sum_{j=1}^{N} A_{ij}^{EI} \int\cdots\int P_n(\phi_j) f^I(\{\phi\};\{J\};t)\; d\phi_1\; d\phi_2 \ldots d\phi_N\; dJ_1\; dJ_2 \ldots dJ_N \tag{52}$$
$$= \frac{1}{N}\sum_{j=1}^{N} A_{ij}^{EI} \int_{-\infty}^{\infty}\int_{0}^{2\pi} P_n(\phi_j) f_j^I(\phi_j, J_j, t) d\phi_j\; dJ_j$$

where $f_j^E(\theta_j, I_j, t)$ is the marginal distribution for θ_j, given by

$$f_j^E(\theta_j, I_j, t) = \int\cdots\int f^E(\{\theta\};\{I\};t) \prod_{k\neq j} d\theta_k\; dI_k \tag{53}$$

and similarly

$$f_j^I(\phi_j, J_j, t) = \int\cdots\int f^I(\{\phi\};\{J\};t) \prod_{k\neq j} d\phi_k\; dJ_k \tag{54}$$

Multiplying the continuity equation (40) by $\prod_{k\neq j} d\theta_k\; dI_k$ and integrating we find that each f_j^E satisfies

$$\frac{\partial f_j^E}{\partial t} + \frac{\partial}{\partial \theta_j}\left[f_j^E \left(\frac{d\theta_j}{dt} \right) \right] = 0 \tag{55}$$

Similarly each f_j^I satisfies

$$\frac{\partial f_j^I}{\partial t} + \frac{\partial}{\partial \phi_j}\left[f_j^I \left(\frac{d\phi_j}{dt} \right) \right] = 0 \tag{56}$$

Using the Ott/Antonsen ansatz we write

$$f_j^E(\theta_j, I_j, t) = \frac{h(I_j)}{2\pi}\left\{ 1 + \sum_{n=1}^{\infty} \left[\alpha_j^E(I_j,t)\right]^n e^{in\theta_j} + c.c. \right\} \tag{57}$$

and

$$f_j^I(\phi_j, J_j, t) = \frac{g(J_j)}{2\pi}\left\{ 1 + \sum_{n=1}^{\infty} \left[\alpha_j^I(J_j,t)\right]^n e^{in\phi_j} + c.c. \right\} \tag{58}$$

for some functions $\alpha_j^E(I_j,t)$ and $\alpha_j^I(J_j,t)$, where "*c.c.*" means the complex conjugate of the previous term. Substituting (57) into (55) and (58) into (56) we find that

$$\frac{\partial \alpha_j^E}{\partial t} = -i\left[\frac{I_j + g_{EE}v_j - g_{EI}s_j - 1}{2} + (I_j + g_{EE}v_j - g_{EI}s_j + 1)\alpha_j^E \right. \tag{59}$$
$$\left. + \frac{I_j + g_{EE}v_j - g_{EI}s_j - 1}{2}\left(\alpha_j^E\right)^2 \right]$$

and

$$\frac{\partial \alpha_j^I}{\partial t} = -i\left[\frac{J_j + g_{IE}u_j - 1}{2} + (J_j + g_{IE}u_j + 1)\alpha_j^I + \frac{J_j + g_{IE}u_j - 1}{2}\left(\alpha_j^I\right)^2 \right] \tag{60}$$

Substituting (57) and (58) into (50)-(52) we obtain

$$q_i = \frac{1}{N}\sum_{j=1}^{N} A_{ij}^{IE} \int_{-\infty}^{\infty} h(I_j) H\left(\alpha_j^E(I_j,t); n\right)\; dI_j \tag{61}$$

$$r_i = \frac{1}{N}\sum_{j=1}^{N} A_{ij}^{EE} \int_{-\infty}^{\infty} h(I_j) H\left(\alpha_j^E(I_j,t);n\right)\ dI_j \tag{62}$$

$$s_i = \frac{1}{N}\sum_{j=1}^{N} A_{ij}^{EI} \int_{-\infty}^{\infty} g(J_j) H\left(\alpha_j^I(J_j,t);n\right)\ dJ_j \tag{63}$$

where H is given by (36). Using standard properties of the Lorentzian one can perform the integrals in (61)-(63) and defining $z_j^E(t) \equiv \bar{\alpha}_j^E(I_0 + i\Delta, t)$ and $z_j^I(t) \equiv \bar{\alpha}_j^I(J_0 + i\Delta, t)$ we have

$$q_i = \frac{1}{N}\sum_{j=1}^{N} A_{ij}^{IE} H\left(z_j^E(t);n\right) \tag{64}$$

$$r_i = \frac{1}{N}\sum_{j=1}^{N} A_{ij}^{EE} H\left(z_j^E(t);n\right) \tag{65}$$

$$s_i = \frac{1}{N}\sum_{j=1}^{N} A_{ij}^{EI} H\left(z_j^I(t);n\right) \tag{66}$$

Evaluating (59) at $I_j = I_0 + i\Delta$ and (60) at $J_j = J_0 + i\Delta$ we obtain

$$\frac{dz_j^E}{dt} = \frac{(iI_0 - \Delta)\left(1 + z_j^E\right)^2 - i\left(1 - z_j^E\right)^2}{2} + \frac{i(1+z_j^E)^2(g_{EE}v_j - g_{EI}s_j)}{2} \tag{67}$$

$$\frac{dz_j^I}{dt} = \frac{(iJ_0 - \Delta)\left(1 + z_j^I\right)^2 - i\left(1 - z_j^I\right)^2}{2} + \frac{i\left(1 + z_j^I\right)^2 g_{IE}u_j}{2} \tag{68}$$

for $j = 1, 2, \ldots N$. Equations (64)-(68) are equations (42)-(46) in Sec. 2.4.

References

[1] D.M. Abrams and S.H. Strogatz. Chimera states for coupled oscillators. *Phys. Rev. Lett.*, 93(17):174102, 2004.

[2] D.M. Abrams and S.H. Strogatz. Chimera states in a ring of nonlocally coupled oscillators. *Int. J. Bifurcat. Chaos*, 16(1):21–37, 2006.

[3] Shun-ichi Amari. Dynamics of pattern formation in lateral-inhibition type neural fields. *Biological cybernetics*, 27(2):77–87, 1977.

[4] Peter Ashwin, Stephen Coombes, and Rachel Nicks. Mathematical frameworks for oscillatory network dynamics in neuroscience. *The Journal of Mathematical Neuroscience*, 6(1):1–92, 2016.

[5] Gilad Barlev, Thomas M. Antonsen, and Edward Ott. The dynamics of network coupled phase oscillators: An ensemble approach. *Chaos*, 21(2):025103, 2011.

[6] Patrick Blomquist, John Wyller, and Gaute T Einevoll. Localized activity patterns in two-population neuronal networks. *Physica D: Nonlinear Phenomena*, 206(3):180–212, 2005.

[7] Christoph Börgers and Nancy Kopell. Effects of noisy drive on rhythms in networks of excitatory and inhibitory neurons. *Neural computation*, 17(3):557–608, 2005.

[8] CA Brackley and Matthew S Turner. Persistent fluctuations of activity in undriven continuum neural field models with power-law connections. *Physical Review E*, 79(1):011918, 2009.

[9] Chris A Brackley and Matthew S Turner. Heterogeneous connectivity in neural fields: A stochastic approach. In Stephen Coombes, Peter beim Graben, Roland Potthast, and James J. Wright, editors, *Neural Fields*, pages 213–234. Springer, 2014.

[10] Paul C Bressloff. Spatiotemporal dynamics of continuum neural fields. *Journal of Physics A: Mathematical and Theoretical*, 45(3):033001, 2012.

[11] Ed Bullmore and Olaf Sporns. Complex brain networks: graph theoretical analysis of structural and functional systems. *Nature Reviews Neuroscience*, 10(3):186–198, 2009.
[12] Marcelo Camperi and Xiao-Jing Wang. A model of visuospatial working memory in prefrontal cortex: recurrent network and cellular bistability. *Journal of computational neuroscience*, 5(4):383–405, 1998.
[13] Albert Compte, Nicolas Brunel, Patricia S. Goldman-Rakic, and Xiao-Jing Wang. Synaptic mechanisms and network dynamics underlying spatial working memory in a cortical network model. *Cerebral Cortex*, 10(9):910–923, 2000.
[14] Stephen Coombes and Áine Byrne. Next generation neural mass models. In A. Torcini and F. Corinth, editors, *Lecture Notes in Nonlinear Dynamics in Computational Neuroscience: from Physics and Biology to ICT*. Springer, 2016.
[15] B. Ermentrout. Neural networks as spatio-temporal pattern-forming systems. *Rep. Prog. Phys.*, 61:353–430, 1998.
[16] Bard Ermentrout. Type i membranes, phase resetting curves, and synchrony. *Neural computation*, 8(5):979–1001, 1996.
[17] Bard Ermentrout. Gap junctions destroy persistent states in excitatory networks. *Physical Review E*, 74(3):031918, 2006.
[18] G. B. Ermentrout and N. Kopell. Parabolic bursting in an excitable system coupled with a slow oscillation. *SIAM Journal on Applied Mathematics*, 46(2):233–253, 1986.
[19] Boris S Gutkin, Carlo R Laing, Carol L Colby, Carson C Chow, and G Bard Ermentrout. Turning on and off with excitation: the role of spike-timing asynchrony and synchrony in sustained neural activity. *Journal of computational neuroscience*, 11(2):121–134, 2001.
[20] C. R. Laing and W.C. Troy. PDE methods for nonlocal models. *SIAM Journal on Applied Dynamical Systems*, 2(3):487–516, 2003.
[21] Carlo R. Laing. The dynamics of chimera states in heterogeneous Kuramoto networks. *Physica D*, 238(16):1569–1588, 2009.
[22] Carlo R Laing. Derivation of a neural field model from a network of theta neurons. *Physical Review E*, 90(1):010901, 2014.
[23] Carlo R Laing. Numerical bifurcation theory for high-dimensional neural models. *The Journal of Mathematical Neuroscience*, 4(1):13, 2014.
[24] Carlo R Laing. Exact neural fields incorporating gap junctions. *SIAM Journal on Applied Dynamical Systems*, 14(4):1899–1929, 2015.
[25] Carlo R. Laing. Phase oscillator network models of brain dynamics. In Ahmed Moustafa, editor, *Computational Models of Brain and Behavior*. Wiley-Blackwell, 2016.
[26] Carlo R Laing. Travelling waves in arrays of delay-coupled phase oscillators. *To appear in Chaos*, 2016.
[27] Carlo R Laing and Carson C Chow. A spiking neuron model for binocular rivalry. *Journal of computational neuroscience*, 12(1):39–53, 2002.
[28] Carlo R Laing, Karthikeyan Rajendran, and Ioannis G Kevrekidis. Chimeras in random non-complete networks of phase oscillators. *Chaos*, 22(1):013132, 2012.
[29] Carlo R Laing, William C Troy, Boris Gutkin, and G Bard Ermentrout. Multiple bumps in a neuronal model of working memory. *SIAM Journal on Applied Mathematics*, 63(1):62–97, 2002.
[30] C.R. Laing and C.C. Chow. Stationary bumps in networks of spiking neurons. *Neural Comput.*, 13(7):1473–1494, 2001.
[31] Tanushree B Luke, Ernest Barreto, and Paul So. Complete classification of the macroscopic behavior of a heterogeneous network of theta neurons. *Neural computation*, 25(12):3207–3234, 2013.
[32] Tanushree B Luke, Ernest Barreto, and Paul So. Macroscopic complexity from an autonomous network of networks of theta neurons. *Frontiers in computational neuroscience*, 8(145), 2014.
[33] Georgi S Medvedev. Small-world networks of kuramoto oscillators. *Physica D: Nonlinear Phenomena*, 266:13–22, 2014.
[34] Ernest Montbrió, Diego Pazó, and Alex Roxin. Macroscopic description for networks of spiking neurons. *Phys. Rev. X*, 5:021028, Jun 2015.
[35] Mark EJ Newman and Duncan J Watts. Renormalization group analysis of the small-world network model. *Physics Letters A*, 263(4):341–346, 1999.
[36] Edward Ott and Thomas M. Antonsen. Low dimensional behavior of large systems of globally coupled oscillators. *Chaos*, 18(3):037113, 2008.
[37] Edward Ott and Thomas M. Antonsen. Long time evolution of phase oscillator systems. *Chaos*, 19(2):023117, 2009.

[38] Edward Ott, Brian R. Hunt, and Thomas M. Antonsen. Comment on "Long time evolution of phase oscillator systems" [Chaos 19, 023117 (2009)]. *Chaos*, 21(2):025112, 2011.

[39] MR Owen, CR Laing, and Stephen Coombes. Bumps and rings in a two-dimensional neural field: splitting and rotational instabilities. *New Journal of Physics*, 9(10):378, 2007.

[40] Mark J Panaggio and Daniel M Abrams. Chimera states: coexistence of coherence and incoherence in networks of coupled oscillators. *Nonlinearity*, 28(3):R67, 2015.

[41] David J Pinto and G Bard Ermentrout. Spatially structured activity in synaptically coupled neuronal networks: Ii. lateral inhibition and standing pulses. *SIAM Journal on Applied Mathematics*, 62(1):226–243, 2001.

[42] Marko Puljic and Robert Kozma. Narrow-band oscillations in probabilistic cellular automata. *Phys. Rev. E*, 78:026214, Aug 2008.

[43] A David Redish, Adam N Elga, and David S Touretzky. A coupled attractor model of the rodent head direction system. *Network: Computation in Neural Systems*, 7(4):671–685, 1996.

[44] Paul So, Tanushree B Luke, and Ernest Barreto. Networks of theta neurons with time-varying excitability: Macroscopic chaos, multistability, and final-state uncertainty. *Physica D: Nonlinear Phenomena*, 267:16–26, 2014.

[45] H Francis Song and Xiao-Jing Wang. Simple, distance-dependent formulation of the Watts-Strogatz model for directed and undirected small-world networks. *Physical Review E*, 90(6):062801, 2014.

[46] S.H. Strogatz. From Kuramoto to Crawford: exploring the onset of synchronization in populations of coupled oscillators. *Physica D*, 143(1-4):1–20, 2000.

[47] Rüdiger Thul, Stephen Coombes, and Carlo R. Laing. Neural field models with threshold noise. *The Journal of Mathematical Neuroscience*, 6(1):1–26, 2016.

[48] Xiao-Jing Wang. Synaptic reverberation underlying mnemonic persistent activity. *Trends in Neurosciences*, 24(8):455 – 463, 2001.

[49] S. Watanabe and S.H. Strogatz. Integrability of a globally coupled oscillator array. *Phys. Rev. Lett.*, 70:2391–2394, 1993.

[50] S. Watanabe and SH Strogatz. Constants of motion for superconducting Josephson arrays. *Physica D*, 74:197–253, 1994.

[51] Duncan J Watts and Steven H Strogatz. Collective dynamics of "small-world" networks. *Nature*, 393(6684):440–442, 1998.

[52] Hugh R Wilson and Jack D Cowan. A mathematical theory of the functional dynamics of cortical and thalamic nervous tissue. *Kybernetik*, 13(2):55–80, 1973.

[53] Klaus Wimmer, Duane Q Nykamp, Christos Constantinidis, and Albert Compte. Bump attractor dynamics in prefrontal cortex explains behavioral precision in spatial working memory. *Nature neuroscience*, 2014.

[54] Kechen Zhang. Representation of spatial orientation by the intrinsic dynamics of the head-direction cell ensemble: a theory. *The journal of neuroscience*, 16(6):2112–2126, 1996.

E-mail address: c.r.laing@massey.ac.nz

Institute of Natural and Mathematical Sciences, Massey University, Private Bag 102-904 NSMC, Auckland, New Zealand., phone: +64-9-414 0800 extn. 43512 fax: +64-9-4418136